

# Osteoprotection by semaphorin 3A

Mikihito Hayashi<sup>1,2,3</sup>, Tomoki Nakashima<sup>1,2,3</sup>, Masahiko Taniguchi<sup>4</sup>, Tatsuhiko Kodama<sup>5</sup>, Atsushi Kumanogoh<sup>6,7</sup> & Hiroshi Takayanagi<sup>1,2,3,8</sup>

**The bony skeleton is maintained by local factors that regulate bone-forming osteoblasts and bone-resorbing osteoclasts, in addition to hormonal activity. Osteoprotegerin protects bone by inhibiting osteoclastic bone resorption, but no factor has yet been identified as a local determinant of bone mass that regulates both osteoclasts and osteoblasts. Here we show that semaphorin 3A (Sema3A) exerts an osteoprotective effect by both suppressing osteoclastic bone resorption and increasing osteoblastic bone formation. The binding of Sema3A to neuropilin-1 (Nrp1) inhibited receptor activator of nuclear factor- $\kappa$ B ligand (RANKL)-induced osteoclast differentiation by inhibiting the immunoreceptor tyrosine-based activation motif (ITAM) and RhoA signalling pathways. In addition, Sema3A and Nrp1 binding stimulated osteoblast and inhibited adipocyte differentiation through the canonical Wnt/ $\beta$ -catenin signalling pathway. The osteopenic phenotype in *Sema3a*<sup>-/-</sup> mice was recapitulated by mice in which the Sema3A-binding site of Nrp1 had been genetically disrupted. Intravenous Sema3A administration in mice increased bone volume and expedited bone regeneration. Thus, Sema3A is a promising new therapeutic agent in bone and joint diseases.**

Bone homeostasis has long been thought to be predominantly maintained by the endocrine system by calcium regulating hormones, but increasing evidence indicates that bone is also under the control of factors related to immune and neuronal regulation<sup>1,2</sup>. As an imbalance between bone resorption and formation results in metabolic bone disorders such as osteoporosis<sup>3,4</sup>, understanding the balancing mechanisms is important for the development of therapeutic agents. Because bone formation is linked to resorption through coupling factors<sup>5,6</sup>, treatment with anti-resorptive agents results in simultaneous suppression of bone formation, with the result that the efficacy is compromised<sup>6-9</sup>. It is thus crucial to identify a molecule that can regulate both resorption and formation synchronously.

Osteoclasts are derived from monocyte/macrophage precursor cells, and their differentiation is regulated by mesenchymal cells, such as osteoblasts, chondrocytes and osteocytes, which express the key osteoclast differentiation factor RANKL<sup>1,10-12</sup>. Osteoblastic cells counterbalance the function of RANKL by producing a soluble decoy receptor for RANKL, osteoprotegerin (Opg), the name of which indicates it is a protector of bone<sup>13</sup>. Here we show that conditioned medium from Opg-deficient mouse calvarial cells contains factors that inhibit osteoclast formation, and one of these factors is the axon guidance molecule Sema3A. Sema3A inhibits osteoclast differentiation and promotes osteoblastic bone formation, and is thus a potent osteoprotective factor produced by osteoblastic cells.

## Sema3A mediates anti-osteoclastogenesis in osteoblasts

The conditioned medium of osteoblastic cells was able to inhibit osteoclast differentiation of bone marrow-derived monocyte/macrophage precursor cells (BMMs) stimulated by RANKL in the presence of macrophage colony-stimulating factor (M-CSF) (Fig. 1a). We observed a substantial anti-osteoclastogenic effect in the conditioned medium of calvarial cells lacking the *Tnfrsf11b* gene (encoding Opg in mice) (Fig. 1a), suggesting the presence of one or more other soluble

inhibitory factors. To identify the osteoblast-secreted proteins that inhibit osteoclast differentiation, we fractionated the conditioned medium of *Tnfrsf11b*<sup>-/-</sup> calvarial cells by anion-exchange liquid chromatography (Fig. 1b). We found that fractions 8–10 exerted a potent inhibitory effect on osteoclast differentiation (Fig. 1b). The proteins in fraction 8 were separated by SDS-polyacrylamide gel electrophoresis (SDS-PAGE; Fig. 1c), and the major bands were excised and analysed by liquid chromatography–tandem mass spectrometry (LC-MS/MS). Among the identified proteins (Fig. 1d), we focused on the axon guidance molecule Sema3A<sup>14,15</sup> (Supplementary Fig. 1a), as recent studies have suggested that axon guidance molecules are involved in the interaction between osteoblasts and osteoclasts<sup>16-18</sup>. Previous reports suggest that Sema3A expressed in the skeletal system may have a role in the regulation of innervation and blood vessel invasion and contribute to skeletal patterning<sup>19-21</sup>, but the function of Sema3A in the regulation of bone remodelling remains unknown.

Western blot analysis confirmed that Sema3A protein was present in fractions 8 and 9 (Supplementary Fig. 1b), and that the inhibitory effect of fraction 9 is largely mediated by Sema3A, as this effect was abrogated by the addition of soluble Nrp1, which functioned as a Sema3A decoy receptor (Supplementary Fig. 1c). The addition of recombinant Sema3A potentially inhibited osteoclast differentiation in a dose-dependent manner when Sema3A was added before RANKL treatment (Fig. 1e). When Sema3A was added after RANKL treatment, the inhibitory effect was not observed (Fig. 1e). *Sema3a* was predominantly expressed in osteoblast lineage cells among various cells examined (Supplementary Fig. 2a), whereas Sema3A was not detected in osteoclasts (Supplementary Fig. 2a–c). The expression of *Sema3a* messenger RNA in isolated osteocytes and osteoblasts was comparable (Supplementary Fig. 2d). *Sema3a* mRNA expression in calvarial cells was higher than that of any other semaphorin family member tested (Supplementary Fig. 2e).

<sup>1</sup>Department of Cell Signaling, Graduate School of Medical and Dental Sciences, Tokyo Medical and Dental University, Yushima 1-5-45, Bunkyo-ku, Tokyo 113-8549, Japan. <sup>2</sup>Japan Science and Technology Agency, Exploratory Research for Advanced Technology Program, Takayanagi Osteonetwork Project, Yushima 1-5-45, Bunkyo-ku, Tokyo 113-8549, Japan. <sup>3</sup>Global Center of Excellence Program, International Research Center for Molecular Science in Tooth and Bone Diseases, Yushima 1-5-45, Bunkyo-ku, Tokyo 113-8549, Japan. <sup>4</sup>Department of Molecular Medical Sciences, Research Institute for Frontier Medicine, Sapporo Medical University School of Medicine, S-1, W-17, Chuo-ku, Sapporo 060-8556, Japan. <sup>5</sup>Laboratory for Systems Biology and Medicine, Research Center for Advanced Science and Technology, Department of Molecular Biology and Medicine, University of Tokyo, Komaba 4-6-1, Meguro-ku, Tokyo 153-8904, Japan. <sup>6</sup>Department of Respiratory Medicine, Allergy and Rheumatic Diseases, Graduate School of Medicine, Osaka University, Yamadaoka 2-2, Suita, Osaka 565-0871, Japan. <sup>7</sup>Department of Immunopathology, Immunology Frontier Research Center, Osaka University, Yamadaoka 3-1, Suita, Osaka 565-0871, Japan. <sup>8</sup>Centre for Orthopaedic Research, School of Surgery, The University of Western Australia, Nedlands, Western Australia 6009, Australia.

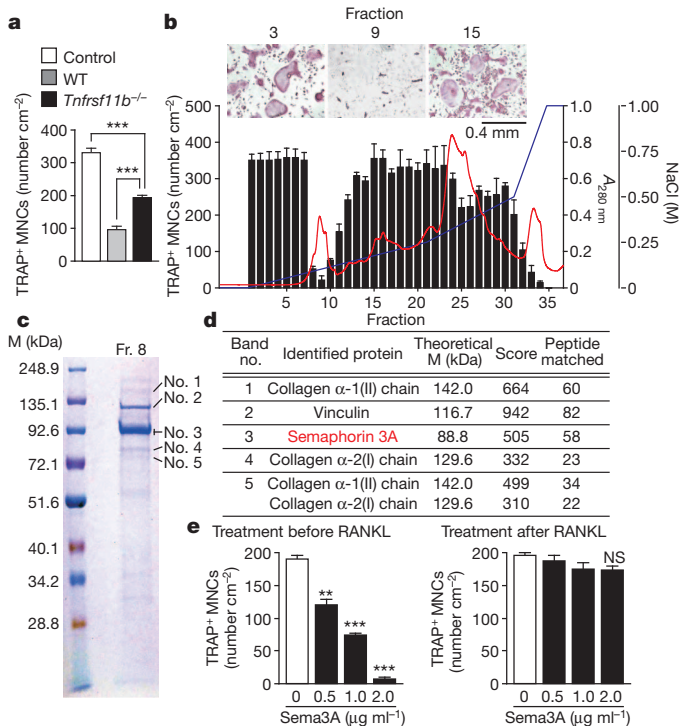


**Figure 1 | Identification of Semaphorin 3A as an inhibitory factor of osteoclast differentiation.** **a**, Effect of wild-type (WT) and Opg-deficient (*Tnfrsf11b*<sup>-/-</sup>) calvarial cell-conditioned medium on osteoclast differentiation. MNC, mononuclear cells. **b**, Fractionation of Opg-deficient calvarial cell-conditioned medium by anion-exchange chromatography, and the effect of each fraction on osteoclast differentiation (black bars). Absorbance at 280 nm is indicated as a red line and the concentration of NaCl as a blue line. Inset shows TRAP staining of osteoclast cultures treated with fractions 3, 9 and 15. **c**, Coomassie brilliant blue-stained SDS-PAGE image of fraction 8. M, molecular mass. **d**, List of the identified proteins (that is, more than 300 on the MASCOT score), their theoretical molecular mass, MASCOT score and the number of non-redundant peptides. **e**, Effect of Semaphorin 3A treatment on osteoclast differentiation. Error bars (**a**, **b** and **e**) denote mean  $\pm$  s.e.m. \*\**P* < 0.01; \*\*\**P* < 0.005; NS, not significant.

### Semaphorin 3A regulates osteoclast differentiation via Nrp1

Microcomputed tomography along with bone morphometric and radiographic analyses showed that *Sema3a*<sup>-/-</sup> mice<sup>19</sup> have a severe osteopenic phenotype both in trabecular and cortical bones, accompanied by an increase in the osteoclast number and eroded surface (Fig. 2a, b and Supplementary Fig. 3a–c). There was no difference in the number of osteoclast precursor CD11b<sup>low/-</sup>CD3ε<sup>-</sup>B220<sup>-</sup>c-fms<sup>+</sup>c-kit<sup>+</sup> cells<sup>22</sup> in the bone marrow of wild-type and *Sema3a*<sup>-/-</sup> mice (Supplementary Fig. 3d).

When osteoclast formation was analysed in a coculture of bone marrow and calvarial cells, the formation of tartrate-resistant acid phosphatase (TRAP)-positive multinucleated osteoclasts was markedly enhanced in *Sema3a*<sup>-/-</sup> cells (Fig. 2c and Supplementary Fig. 3e, f). This enhanced osteoclastogenesis was not observed when BMMs were stimulated by RANKL and M-CSF (Supplementary Fig. 3g). In addition, enhanced osteoclastogenesis was observed in the coculture of wild-type bone marrow cells and *Sema3a*<sup>-/-</sup> calvarial cells, but not in the coculture of *Sema3a*<sup>-/-</sup> bone marrow cells and wild-type calvarial cells (Fig. 2c and Supplementary Fig. 3e, f). These results indicate that the osteoblastic expression of Semaphorin 3A inhibits osteoclastogenesis. The level of RANKL and Opg in the calvarial cells or the serum was not affected by Semaphorin 3A deficiency (Supplementary Fig. 3h, i).

Semaphorin 3A binds to a receptor complex of the ligand-binding subunit Nrp1 and one of the class A plexins (PlxnA1, PlxnA2, PlxnA3 and PlxnA4), which function as the signal-transducing subunit<sup>23</sup>. We found that Nrp1 expression in BMMs was rapidly and markedly

suppressed after RANKL stimulation (Fig. 2d). Because Semaphorin 3A-induced inhibition of osteoclastogenesis was observed only when Semaphorin 3A was added before RANKL stimulation (Fig. 1e), we proposed that Semaphorin 3A does not inhibit osteoclastogenesis after RANKL stimulation owing to Nrp1 downregulation.

When Nrp1 was overexpressed by retroviral transfer, Semaphorin 3A exerted an inhibitory effect even when Semaphorin 3A had been added after RANKL stimulation (Supplementary Fig. 3j). Notably, osteoclastogenesis was inhibited by Nrp1 overexpression only (Supplementary Fig. 3j). When *Nrp1* expression was knocked down by short hairpin RNA (shRNA), the inhibitory effect of Semaphorin 3A on osteoclast differentiation was abolished (Supplementary Fig. 3k). Thus, the level of Nrp1 correlates with the inhibitory effect of Semaphorin 3A on osteoclastogenesis, suggesting that the Nrp1 downregulation caused by RANKL signalling is important for proper osteoclast differentiation by cancelling the inhibitory effect of Semaphorin 3A.

Furthermore, we analysed knockin mice in which the *Nrp1* gene was replaced by mutant *Nrp1* lacking the Semaphorin-binding site (*Nrp1*<sup>Sema-</sup> mice), as *Nrp1*<sup>-/-</sup> mice are embryonically lethal and Nrp1 also contains the vascular endothelial growth factor (VEGF)-binding site<sup>24</sup>. Semaphorin 3A did not inhibit RANKL-induced osteoclast differentiation in *Nrp1*<sup>Sema-</sup> cells (Supplementary Fig. 3l), showing that Semaphorin 3A inhibits osteoclastogenesis by binding to Nrp1. As expected, *Nrp1*<sup>Sema-</sup> mice showed an osteopenic phenotype accompanied by enhanced osteoclast differentiation, which was similar to *Sema3a*<sup>-/-</sup> mice (Fig. 2e, f and Supplementary Fig. 3m–o).

To understand the mechanism of the RANKL-induced inhibition of Nrp1 expression, we examined the involvement of the transcription factors nuclear factor- $\kappa$ B (NF- $\kappa$ B), c-Fos and nuclear factor of activated T cells c1 (NFATc1), which are all activated by RANKL<sup>1</sup>. RANKL-induced downregulation of *Nrp1* expression was abolished by an NF- $\kappa$ B inhibitor, but was not affected by the deficiency of NFATc1 or c-Fos (Supplementary Fig. 4a–c). Chromatin immunoprecipitation analysis showed that NF- $\kappa$ B p65 and, to a lesser extent, p50 were recruited to the proximal NF- $\kappa$ B-binding site of the *Nrp1* promoter after RANKL stimulation (Supplementary Fig. 4d, e). NF- $\kappa$ B p65 and p50 inhibited *Nrp1* promoter activity in a reporter gene assay (Supplementary Fig. 4f). Retroviral overexpression of p65 in BMMs led to Nrp1 downregulation in the absence of RANKL, which was further facilitated by p50 overexpression (Supplementary Fig. 4g). These effects were dependent on histone deacetylases (Supplementary Fig. 4g, h), suggesting that the recruitment of corepressors<sup>25</sup> by RANKL-stimulated NF- $\kappa$ B is involved in Nrp1 downregulation.

### Mechanism of anti-osteoclastogenesis by Semaphorin 3A

The binding of RANKL to its receptor RANK results in the activation of tumour-necrosis factor (TNF) receptor-associated factor 6 (TRAF6), which stimulates the NF- $\kappa$ B and mitogen-activated protein kinase (MAPK) pathways<sup>1</sup>. RANKL also activates the activator protein 1 (AP-1) transcription factor complex, including c-Fos, which cooperates with NF- $\kappa$ B to induce NFATc1, thus activating the transcription of osteoclast-specific genes<sup>1,26</sup>. The robust induction of NFATc1 is dependent on calcium signalling (costimulatory signalling) stimulated by the ITAM-bearing adaptor molecules DNAX-activation protein 12 (DAP12) and Fc receptor common  $\gamma$  subunit (FcR $\gamma$ ), which associate with immunoglobulin-like receptors such as triggering receptor expressed on myeloid cells 2 (TREM2) and osteoclast-associated receptor (OSCAR)<sup>1,27</sup>.

From these observations, the question arises as to how the Semaphorin 3A–Nrp1 axis inhibits osteoclastogenic signalling. RANKL-stimulated induction of the osteoclastic genes *Ctsk*, *Acp5* and *Nfatc1* was severely impaired by Semaphorin 3A without affecting the expression of *Tnfrsf11a* or *Csf1r* (Fig. 3a). There was no difference in the cell proliferation rate or the percentage of apoptotic cells among the osteoclast precursor cells between the Semaphorin 3A-treated and the control cells (Supplementary Fig. 5a, b). RANKL-induced activation

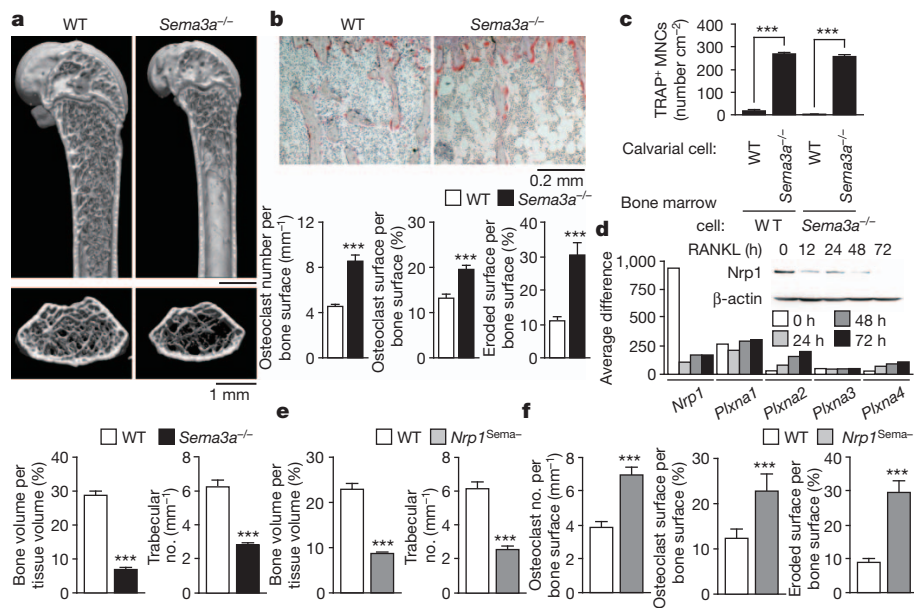


**Figure 2 | *Sema3a*<sup>-/-</sup> and *Nrpl1*<sup>Sema-</sup> mice show a severe low bone mass phenotype.**

**a**, Microcomputed tomography images of the femurs of 10-week-old *Sema3a*<sup>-/-</sup> mice and their wild-type littermates (*n* = 4–6). The bone volume and parameters of trabecular bone were determined by microcomputed tomography analysis. **b**, TRAP staining of the proximal tibiae of *Sema3a*<sup>-/-</sup> mice and their wild-type littermates (*n* = 4–6). Osteoclastic parameters were measured using bone morphometric analysis. **c**, Osteoclast differentiation from wild-type or *Sema3a*<sup>-/-</sup> bone marrow cells in coculture with wild-type or *Sema3a*<sup>-/-</sup> calvarial cells at day 4. **d**, GeneChip analysis of the mRNA expression of *Nrpl1* and *Plxn1–4* during osteoclast differentiation. *Nrpl1* protein expression in BMMs stimulated with RANKL was analysed by western blot (inset). **e**, Microcomputed tomography analysis of the femurs of 10-week-old *Nrpl1*<sup>Sema-</sup> mice and their wild-type littermates (*n* = 4–5). **f**, Parameters for osteoclastic bone resorption in the bone morphometric analysis of the proximal tibiae of *Nrpl1*<sup>Sema-</sup> mice and their wild-type littermates (*n* = 4–5). Error bars (**a–c**, **e** and **f**) denote mean ± s.e.m. \*\*\**P* < 0.01; \*\*\*\**P* < 0.005.

of the signalling pathways downstream of TRAF6, including the MAPKs (such as ERK, JNK, p38) and inhibitor of κB (IκB) kinases, was comparable in BMMs with or without *Sema3A* (Supplementary Fig. 5c).

*PlxnA1* promotes osteoclast differentiation by activating the ITAM signal through the formation of the *PlxnA1*–*TREM2*–*DAP12* complex in response to ligands such as *Sema6D*<sup>17</sup>. However, *PlxnA1* is constitutively associated with *Nrpl1*, which mediates *Sema3A* signalling

instead of *TREM2*–*DAP12* signalling<sup>28</sup>. With increasing *Nrpl1* expression, the amount of *TREM2* associated with *PlxnA1* decreased and *Nrpl1* associated with *PlxnA1* increased (Fig. 3b).

*RANKL* induced the formation of the *PlxnA1*–*TREM2*–*DAP12* complex by the downregulation of *Nrpl1*, thereby releasing *PlxnA1* from the *PlxnA1*–*Nrpl1* complex (Fig. 3c). *Sema3A* treatment inhibited *RANKL*-induced formation of the *PlxnA1*–*TREM2*–*DAP12* complex by inhibiting *Nrpl1* downregulation and maintaining the *PlxnA1*–*Nrpl1* complex (Fig. 3c). The cell surface and intracellular expression of *Nrpl1* was highly downregulated by *RANKL* treatment (Supplementary Fig. 5d), but *Sema3A* treatment induced the internalization of *Nrpl1*, as already reported<sup>29</sup>, and protected *RANKL*-induced *Nrpl1* downregulation without altering *Nrpl1* mRNA expression (Supplementary Fig. 5d, e).

*RANKL*-induced tyrosine phosphorylation of phospholipase *Cγ2* (*PLCγ2*) and calcium oscillation were both markedly blocked by *Sema3A* treatment (Supplementary Fig. 5f, g). We observed that osteoclast differentiation in *DAP12*-deficient (also known as *Tyrbp*-deficient) bone marrow cells was not enhanced even in a coculture with *Sema3a*<sup>-/-</sup> calvarial cells (Supplementary Fig. 5h), suggesting that *Sema3A*-induced inhibition is mediated by the modulation of *DAP12*-induced ITAM signalling. Thus, *Nrpl1* competes with *TREM2* for *PlxnA1*, thereby functioning as a suppressor of the *PlxnA1*–*TREM2*–*DAP12*-induced costimulatory signal. *Sema3A*-induced inhibition of osteoclast differentiation was less observed in the presence of *Sema6D* (Supplementary Fig. 5i).

We examined the effect of *Sema3A* on the migration of BMMs because the semaphorin–plexin system regulates actin cytoskeletal rearrangement<sup>15,23</sup>. We observed a repulsive effect of *Sema3A* on M-CSF-induced migration of BMMs (Fig. 3d). By contrast, this repulsive effect was not observed in *Nrpl1*<sup>Sema-</sup> BMMs (Fig. 3d). Because semaphorin–plexin signalling regulates the Rho family of small GTPases<sup>15,23</sup>, we examined the effect of *Sema3A* treatment on M-CSF-induced activation of the RhoA and Rac GTPases. *Sema3A* treatment abrogated RhoA activation in response to M-CSF (Fig. 3e), but not Rac activation (Supplementary Fig. 5j), suggesting that the inhibition of RhoA activation is involved in the inhibitory effect of *Sema3A* on the migration of BMMs.

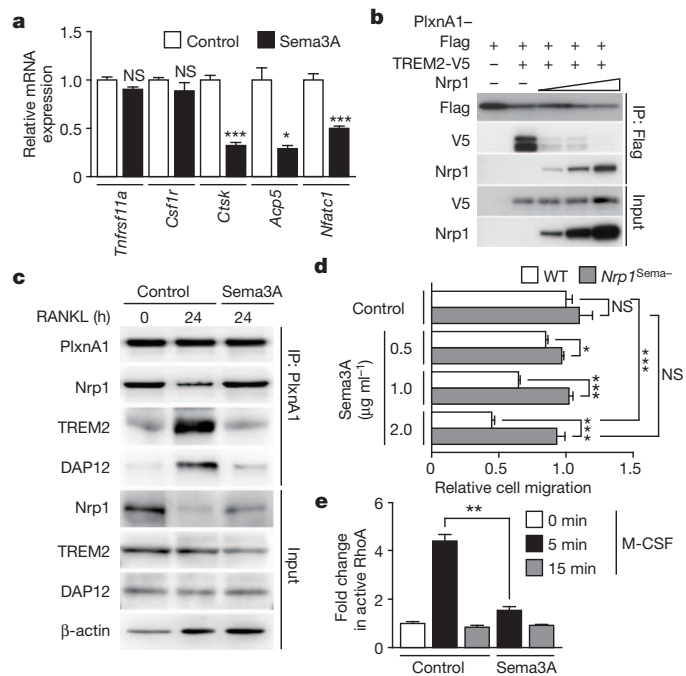


**Figure 3 | Inhibition of osteoclast differentiation by *Sema3A*–*Nrpl1* signalling.** **a**, Effect of *Sema3A* treatment on osteoclastic gene expression in BMMs treated with *RANKL* for 2 days. **b**, Effect of *Nrpl1* expression on the association of *PlxnA1* with *TREM2*. IP, immunoprecipitation. **c**, Effect of *Sema3A* treatment on the formation of a complex of *PlxnA1* with *Nrpl1* or *TREM2*/*DAP12* in *RANKL*-treated BMMs. **d**, Transwell assay of the effect of *Sema3A* on M-CSF-induced migration of BMMs derived from wild-type or *Nrpl1*<sup>Sema-</sup> mice. **e**, Effect of *Sema3A* treatment on the activation of RhoA in BMMs stimulated with M-CSF. Error bars (**a**, **d** and **e**) denote mean ± s.e.m. \**P* < 0.05; \*\**P* < 0.01; \*\*\**P* < 0.005.

**Sema3A regulates osteoblasts through the Wnt pathway**

In addition to an osteoclastic phenotype, both *Sema3a*<sup>-/-</sup> and *Nrpl1*<sup>Sema-</sup> mice were found to have osteoblastic and adipocytic

phenotypes (Fig. 4a and Supplementary Fig. 6a–c); that is, they had a decreased osteoblast number, a reduced bone formation rate and a markedly increased adipocyte number (Fig. 4b and Supplementary Fig. 6d, e) without any significant difference in the weight of the epididymal white adipose tissue per body weight (Supplementary Fig. 6f, g). Taken together, the severe osteopenic phenotype in *Sema3a*<sup>-/-</sup> and *Nrp1*<sup>Sema3a</sup> mice was caused by both a decrease in the osteoblastic bone formation and an increase in osteoclastic bone resorption.

Calvarial cells obtained from *Sema3a*<sup>-/-</sup> or *Nrp1*<sup>Sema3a</sup> mice were cultured in an osteogenic medium with or without Sema3A. Alkaline phosphatase activity and bone nodule formation were markedly decreased in *Sema3a*<sup>-/-</sup> and *Nrp1*<sup>Sema3a</sup> cells, and Sema3A treatment facilitated the differentiation of *Sema3a*<sup>-/-</sup> calvarial cells into osteoblastic cells, but not *Nrp1*<sup>Sema3a</sup> cells (Fig. 4c, d and Supplementary Fig. 6h–k). Neither the cell proliferation rate nor the percentage of apoptotic cells was affected in both types of mutant cells (Supplementary Fig. 6l, m). Adipocyte differentiation was highly increased in both *Sema3a*<sup>-/-</sup> and *Nrp1*<sup>Sema3a</sup> cells, and Sema3A treatment blocked the differentiation of wild-type and *Sema3a*<sup>-/-</sup> cells into adipocytes, but not *Nrp1*<sup>Sema3a</sup> cells (Fig. 4e and Supplementary Fig. 6n, o). In *Sema3a*<sup>-/-</sup> cells, the expression of the osteoblast genes *Runx2*, *Sp7* (which encodes osterix), *Apl1* and *Bglap* (encoding osteocalcin) was strongly suppressed (Supplementary Fig. 7a), and the expression of the adipocyte genes *Pparg*, *Cebpa*, *Fabp4* (encoding aP2) and *Lpl* (encoding lipoprotein lipase) was highly increased (Supplementary Fig. 7b). These results indicate that Sema3A activates osteoblast differentiation and inhibits adipocyte differentiation through Nrp1.

Because the mRNA expression levels of the known regulators of mesenchymal cell differentiation<sup>30,31</sup> were comparable in wild-type and *Sema3a*<sup>-/-</sup> cells (Supplementary Fig. 7c), we performed gene

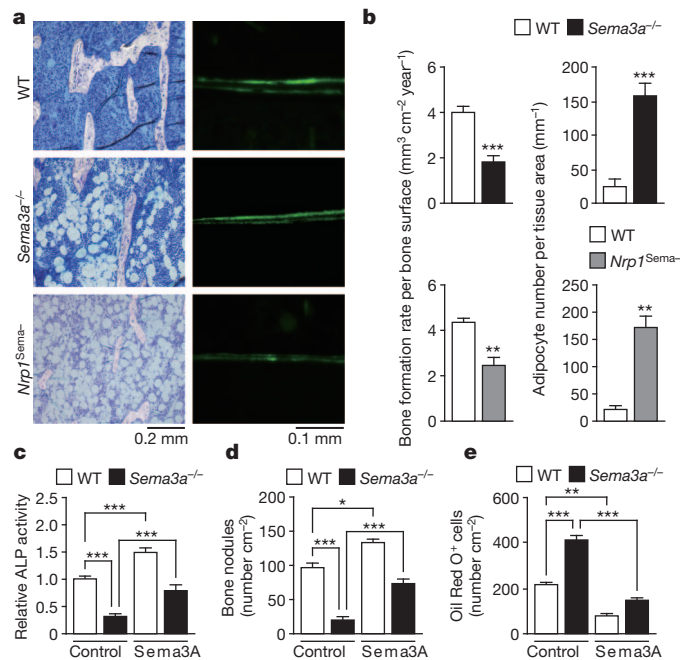


**Figure 4 | Impaired osteoblast differentiation and increased adipocyte differentiation in *Sema3a*<sup>-/-</sup> and *Nrp1*<sup>Sema3a</sup> mice.** **a**, Toluidine blue staining of the proximal tibiae of wild-type, *Sema3a*<sup>-/-</sup> and *Nrp1*<sup>Sema3a</sup> mice (left). New bone formation was determined by calcein double labelling (right).

**b**, Osteoblastic and adipocytic parameters measured by histomorphometric analysis of wild-type, *Sema3a*<sup>-/-</sup> and *Nrp1*<sup>Sema3a</sup> mice ( $n = 4-6$ ). **c**, Alkaline phosphatase (ALP) staining of wild-type and *Sema3a*<sup>-/-</sup> calvarial cells cultured in osteogenic medium with or without Sema3A. **d**, Bone nodule formation in wild-type and *Sema3a*<sup>-/-</sup> calvarial cells cultured in osteogenic medium with or without Sema3A. **e**, Adipocyte differentiation in wild-type and *Sema3a*<sup>-/-</sup> bone marrow stromal cells cultured in adipogenic medium with or without Sema3A. Error bars (b–e) denote mean  $\pm$  s.e.m. \* $P < 0.05$ ; \*\* $P < 0.01$ ; \*\*\* $P < 0.005$ .

expression profiling of the calvarial cells derived from *Sema3a*<sup>-/-</sup> mice to obtain insight into the Sema3A-activated molecular pathways in osteoblasts. Gene set enrichment analysis in *Sema3a*<sup>-/-</sup> cells showed a significant downregulation of the gene sets involved in the Wnt signalling pathway and the Wnt-related signalling pathways (Supplementary Fig. 7d and Supplementary Table 1). We therefore focused on the canonical Wnt pathway, as it is known to promote osteoblast differentiation and inhibit adipocyte differentiation<sup>31-33</sup>. The mRNA expression of most of the transcriptional targets of  $\beta$ -catenin was considerably reduced (Supplementary Fig. 7e), and the Wnt3a-induced nuclear accumulation of  $\beta$ -catenin was suppressed in *Sema3a*<sup>-/-</sup> calvarial cells (Fig. 5a).

The Sema3A signalling pathway induces activation of the small G protein Rac1 through FARP2 (FERM, RhoGEF and pleckstrin domain protein 2), which is a guanyl-nucleotide exchange factor (GEF) specific for Rac1 (ref. 34). Previous studies suggested a regulatory role of FARP2 in transduction of semaphorin-induced repulsive cues in axons, via Rac1 activation<sup>34</sup>. Because Rac1 promotes the nuclear localization of  $\beta$ -catenin in response to canonical Wnt ligands<sup>35</sup>, we examined the activation of Rac proteins and RhoA in *Sema3a*<sup>-/-</sup> cells. The activation of Rac, but not RhoA, in *Sema3a*<sup>-/-</sup> calvarial cells in response to Wnt3a treatment was significantly decreased (Fig. 5b and Supplementary Fig. 7f) as compared with that in wild-type control cells. In addition, Sema3A treatment facilitated the nuclear translocation of  $\beta$ -catenin and the activation of Rac in *Sema3a*<sup>-/-</sup> cells (Fig. 5a, b). The ectopic expression of a dominant negative form of FARP2 ( $\Delta$ GEF-FARP2)<sup>36</sup> in calvarial cells resulted in the inhibition of osteoblast differentiation, even in the presence of Sema3A (Fig. 5c and Supplementary Fig. 7g). When  $\Delta$ GEF-FARP2 was overexpressed, reduced nuclear accumulation of  $\beta$ -catenin was observed and Sema3A treatment had no effect on its nuclear localization (Fig. 5d). These results indicate that Sema3A stimulates the canonical Wnt/ $\beta$ -catenin signalling pathway, at least in part, through FARP2-mediated activation of Rac1 during osteoblast differentiation.

### Sema3A as an osteoprotective therapeutic agent

To determine the *in vivo* effect of Sema3A administration on bone metabolism, 5-week-old male mice were intravenously injected with recombinant Sema3A or saline once a week. After four weeks of treatment, the trabecular bone volume and trabecular parameters in the distal femur were increased in the Sema3A-treated mice (Fig. 6a and Supplementary Fig. 8a). Bone morphometric analysis showed a decrease in osteoclastic parameters and an increase in osteoblastic parameters (Fig. 6b, c and Supplementary Fig. 8b–e), suggesting that Sema3A exerts a bone-increasing effect by stimulating osteoblastic bone formation and inhibiting osteoclastic bone resorption synchronously. We could not detect any pathological findings in vital organs or any behavioural abnormalities after the Sema3A injection (data not shown). The number of osteoclast precursor cells and osteoprogenitor cells in the bone marrow was not influenced by Sema3A administration (Supplementary Fig. 8f and data not shown), but bone marrow mesenchymal cells derived from Sema3A-treated mice tended to differentiate into osteoblasts instead of adipocytes *in vitro*, although the number of colony forming units was unchanged (Supplementary Fig. 8g, h).

We further investigated the therapeutic potential of Sema3A in a bone regeneration model of cortical bone defects induced by drill hole injury<sup>37</sup>. Microcomputed tomography analysis showed that the regenerated cortical bone volume in Sema3A-treated mice was higher than in saline-treated mice (Fig. 6d and Supplementary Fig. 8i). The significantly increased osteoblast surface and decreased osteoclast surface around the injured region were observed by histomorphometric analysis (Fig. 6e). These results indicate that the local administration of Sema3A into the injured site accelerates bone regeneration, although we cannot rule out the possibility that Sema3A exerted a bone protective effect partly through the regulation of innervation.

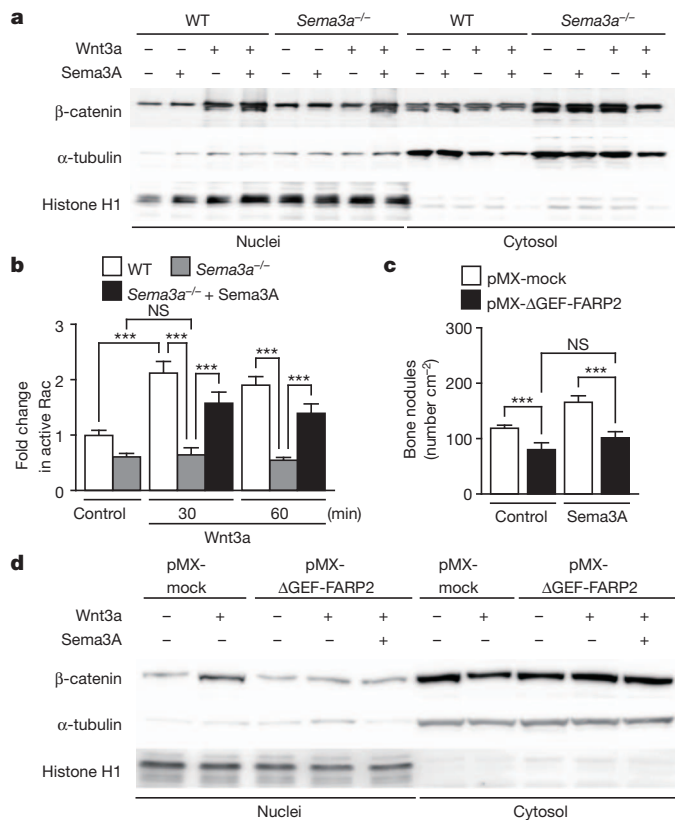


**Figure 5 | Regulation of osteoblast differentiation by Sema3A through canonical Wnt signalling.** **a**, Analysis of nuclear  $\beta$ -catenin levels in the wild-type and *Sema3A*<sup>-/-</sup> calvarial cells stimulated by Wnt3a in the presence or absence of Sema3A. Sema3A was simultaneously added with Wnt3a. **b**, Effect of Sema3A treatment on the activation of Rac in the wild-type and *Sema3A*<sup>-/-</sup> calvarial cells treated with Wnt3a. **c**, Effect of retrovirus-mediated overexpression of  $\Delta$ GEF-FARP2 on bone nodule formation in calvarial cells cultured in the osteogenic medium in the presence or absence of Sema3A. **d**, Effect of retrovirus-mediated overexpression of  $\Delta$ GEF-FARP2 on the nuclear localization of  $\beta$ -catenin in calvarial cells treated with Wnt3a in the presence or absence of Sema3A. Error bars (b, c) denote mean  $\pm$  s.e.m. \*\*\* $P < 0.005$ .

We examined the effect of Sema3A administration on bone loss in an ovariectomized mouse model of postmenopausal osteoporosis. Ovariectomized 9-week-old mice were treated with a weekly intravenous injection of Sema3A starting two days after ovariectomy and continuing for four weeks. Sema3A administration decreased bone loss after ovariectomy both by inhibiting osteoclastic bone resorption and promoting osteoblastic bone formation (Fig. 6f, g and Supplementary Fig. 8j–l). Recombinant human SEMA3A suppressed osteoclastogenesis and promoted osteoblastogenesis in cultured human cells (Supplementary Fig. 9a, b). These results indicate that Sema3A is a promising potential therapeutic target for bone diseases.

## Conclusions

This study demonstrates that the Sema3A expressed by osteoblast lineage cells functions as a potent osteoprotective factor by synchronously inhibiting bone resorption and promoting bone formation (Supplementary Fig. 10a–c). Sema3A represents the long sought soluble molecule with the capacity to bring both osteoblasts and osteoclasts into a condition that favours bone mineral increase. Bone remodelling consists of resorption, transition and formation phases, and the transition phase is under the control of classical coupling factors such as insulin-like growth factor and transforming growth factor- $\beta$ , which link bone resorption with formation<sup>38,39</sup>. Sema3A may have a crucial role in the bone formation phase, in which osteoblasts extensively produce bone, and at the same time restrain osteoclasts from

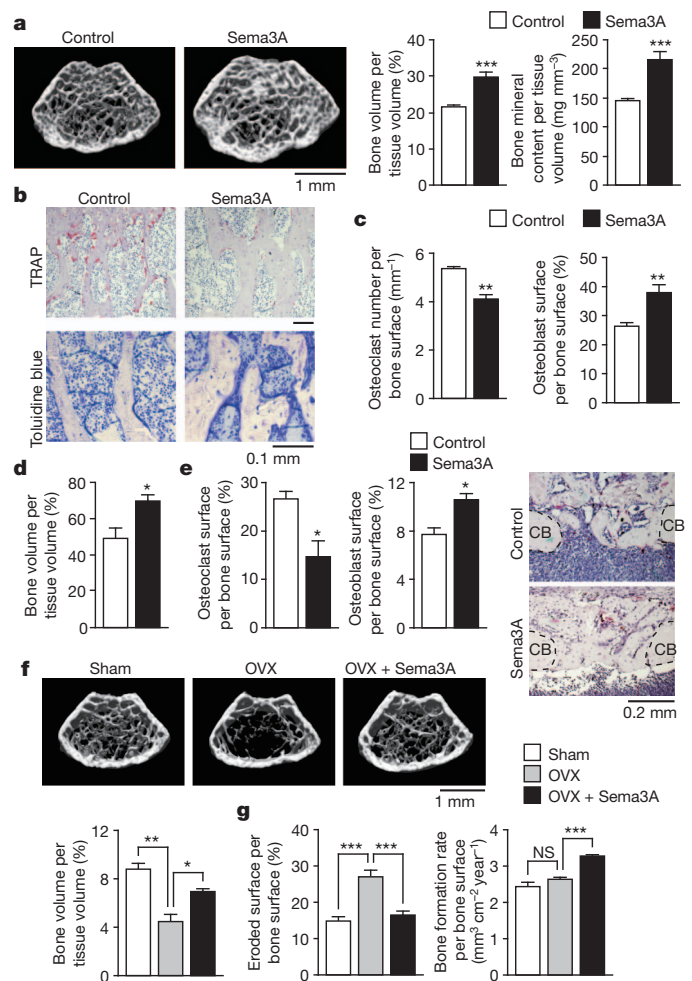


**Figure 6 | Sema3A as a potential bone-increasing agent.** **a**, Microcomputed tomography analysis of the femurs of 9-week-old wild-type mice treated with Sema3A or saline control ( $n = 4-7$ ). **b**, Histological analysis of the proximal tibiae of wild-type mice treated with Sema3A or saline control. **c**, Parameters for osteoclasts and osteoblasts in the bone morphometric analysis of wild-type mice treated with Sema3A or saline control ( $n = 4-7$ ). **d**, Microcomputed tomography analysis of bone regeneration of femoral cortex after drill-hole injury ( $n = 5$ ). **e**, Histomorphometric analysis of the injured site of the femur (TRAP and haematoxylin staining;  $n = 5$ ). CB, cortical bone. **f**, Microcomputed tomography analysis of the femurs of the sham-operated (Sham), ovariectomized (OVX) and Sema3A-treated OVX mice ( $n = 4-5$ ). **g**, Parameters for osteoclastic bone resorption and osteoblastic bone formation in the bone morphometric analysis of the Sham, OVX and Sema3A-treated OVX mice ( $n = 4-5$ ). Error bars (a, c–g) denote mean  $\pm$  s.e.m. \* $P < 0.05$ ; \*\* $P < 0.01$ ; \*\*\* $P < 0.005$ .

migrating to the formation sites and starting to resorb the newly formed bone. The Sema3A protein level in the serum or bone microenvironment could be an auspicious biomarker for bone turnover, as we observed that the serum level of Sema3A decreased with age in mice (data not shown).

The potent anti-osteoclastogenic function of Sema3A is tightly controlled by Nrp1 expression regulated by RANKL signalling. Unless Nrp1 is downregulated by RANKL, the Sema3A–Nrp1 axis inhibits osteoclast differentiation by sequestering PlxnA1 from TREM2 so as to suppress ITAM signalling, and also inhibits RhoA activation via Nrp1–PlxnA to suppress osteoclast precursor cell migration (Supplementary Fig. 10b). After RANKL reduces Nrp1 expression, PlxnA1 associates with TREM2 and DAP12, which facilitate the ITAM-mediated calcium signalling required for osteoclast differentiation (Supplementary Fig. 10b). Because PlxnA1, PlxnA2 and PlxnA3, but not PlxnA4, are expressed by osteoclast and osteoblast

lineage cells (data not shown), the relative contribution of these receptor components should be explored in the future.

Therapeutic agents capable of increasing bone formation have essentially been unavailable except for parathyroid hormone or anti-sclerostin antibody<sup>40</sup>. This study may provide a molecular basis for the development of a combined anti-resorptive and bone-increasing agent capable of facilitating bone regeneration.

## METHODS SUMMARY

**Mice and bone analysis.** The generation of *Sema3a*<sup>-/-</sup>, *Nrp1*<sup>Sema-</sup>, *Fos*<sup>-/-</sup>, *Nfatc1*<sup>-/-</sup>, *Tnfrsf11b*<sup>-/-</sup> and *Tyropb*<sup>-/-</sup> mice was described previously<sup>19,24,41–44</sup>. All mice were maintained under specific pathogen-free conditions. All animal experiments were approved by the Institutional Animal Care and Use Committee of Tokyo Medical and Dental University. Three-dimensional micro-computed tomography analyses and bone morphometric analyses were performed as described<sup>11,14,30,45</sup>. The radiographs were obtained with a high-resolution soft X-ray system (SOFTEX).

**Quantitative RT-PCR analysis and GeneChip analysis.** Real-time quantitative PCR with reverse transcription (RT-PCR) analysis was performed as described<sup>11,14,30,45</sup>. In brief, total RNA was extracted by ISOGEN (NIPPON GENE) according to the manufacturer's instructions. First-strand complementary DNAs were synthesized using Superscript III reverse transcriptase (Invitrogen). Quantitative RT-PCR analysis was performed with the LightCycler apparatus (Roche Applied Science) using SYBR Green Realtime PCR Master Mix (TOYOBO). All primer sequences are available on request. GeneChip analysis and gene set enrichment analysis were performed as described previously<sup>46</sup>.

**Full Methods** and any associated references are available in the online version of the paper at [www.nature.com/nature](http://www.nature.com/nature).

Received 11 November 2011; accepted 27 February 2012.

Published online 18 April 2012.

1. Takayanagi, H. Osteoimmunology: shared mechanisms and crosstalk between the immune and bone systems. *Nature Rev. Immunol.* **7**, 292–304 (2007).
2. Elefteriou, F. Regulation of bone remodeling by the central and peripheral nervous system. *Arch. Biochem. Biophys.* **473**, 231–236 (2008).
3. Seeman, E. & Delmas, P. D. Bone quality—the material and structural basis of bone strength and fragility. *N. Engl. J. Med.* **354**, 2250–2261 (2006).
4. Teitelbaum, S. L. & Ross, F. P. Genetic regulation of osteoclast development and function. *Nature Rev. Genet.* **4**, 638–649 (2003).
5. Martin, T. J. & Sims, N. Osteoclast-derived activity in the coupling of bone formation to resorption. *Trends Mol. Med.* **11**, 76–81 (2005).
6. Lewiecki, E. M. New targets for intervention in the treatment of postmenopausal osteoporosis. *Nature Rev. Rheumatol.* **7**, 631–638 (2011).
7. Rachner, T. D., Khosla, S. & Hofbauer, L. C. Osteoporosis: now and the future. *Lancet* **377**, 1276–1287 (2011).
8. Reid, I. R. *et al.* Effects of denosumab on bone histomorphometry: the FREEDOM and STAND studies. *J. Bone Miner. Res.* **25**, 2256–2265 (2010).
9. Odvina, C. V. *et al.* Severely suppressed bone turnover: a potential complication of alendronate therapy. *J. Clin. Endocrinol. Metab.* **90**, 1294–1301 (2005).
10. Suda, T. *et al.* Modulation of osteoclast differentiation and function by the new members of the tumor necrosis factor receptor and ligand families. *Endocr. Rev.* **20**, 345–357 (1999).
11. Nakashima, T. *et al.* Evidence for osteocyte regulation of bone homeostasis through RANKL expression. *Nature Med.* **17**, 1231–1234 (2011).
12. Xiong, J. *et al.* Matrix-embedded cells control osteoclast formation. *Nature Med.* **17**, 1235–1241 (2011).
13. Simonet, W. S. *et al.* Osteoprotegerin: a novel secreted protein involved in the regulation of bone density. *Cell* **89**, 309–319 (1997).
14. Luo, Y., Raible, D. & Raper, J. A. Collapsin: A protein in brain that induces the collapse and paralysis of neuronal growth cones. *Cell* **75**, 217–227 (1993).
15. Tran, T. S., Kolodkin, A. L. & Bharadwaj, R. Semaphorin regulation of cellular morphology. *Annu. Rev. Cell Dev. Biol.* **23**, 263–292 (2007).
16. Negishi-Koga, T. *et al.* Suppression of bone formation by osteoclastic expression of semaphorin 4D. *Nature Med.* **17**, 1473–1480 (2011).
17. Takegahara, N. *et al.* Plexin-A1 and its interaction with DAP12 in immune responses and bone homeostasis. *Nature Cell Biol.* **8**, 615–622 (2006).
18. Matsuo, K. & Irie, N. Osteoclast-osteoblast communication. *Arch. Biochem. Biophys.* **473**, 201–209 (2008).
19. Taniguchi, M. *et al.* Disruption of *semaphorin III/D* gene causes severe abnormality in peripheral nerve projection. *Neuron* **19**, 519–530 (1997).
20. Gomez, C. *et al.* Expression of Semaphorin-3A and its receptors in endochondral ossification: potential role in skeletal development and innervation. *Dev. Dyn.* **234**, 393–403 (2005).
21. Behar, O., Golden, J. A., Mashimo, H., Schoen, F. J. & Fishman, M. C. Semaphorin III is needed for normal patterning and growth of nerves, bones and heart. *Nature* **383**, 525–528 (1996).

22. Jacquin, C., Gran, D. E., Lee, S. K., Lorenzo, J. A. & Aguila, H. L. Identification of multiple osteoclast precursor populations in murine bone marrow. *J. Bone Miner. Res.* **21**, 67–77 (2006).
23. Neufeld, G. & Kessler, O. The semaphorins: versatile regulators of tumour progression and tumour angiogenesis. *Nature Rev. Cancer* **8**, 632–645 (2008).
24. Gu, C. *et al.* Neuropilin-1 conveys semaphorin and VEGF signaling during neural and cardiovascular development. *Dev. Cell* **5**, 45–57 (2003).
25. Ashburner, B. P., Westerheide, S. D. & Baldwin, A. S. Jr. The p65 (RelA) subunit of NF- $\kappa$ B interacts with the histone deacetylase (HDAC) corepressors HDAC1 and HDAC2 to negatively regulate gene expression. *Mol. Cell Biol.* **21**, 7065–7077 (2001).
26. Takayanagi, H. *et al.* Induction and activation of the transcription factor NFATc1 (NFAT2) integrate RANKL signaling in terminal differentiation of osteoclasts. *Dev. Cell* **3**, 889–901 (2002).
27. Koga, T. *et al.* Costimulatory signals mediated by the ITAM motif cooperate with RANKL for bone homeostasis. *Nature* **428**, 758–763 (2004).
28. Takahashi, T. & Strittmatter, S. M. Plexin1 autoinhibition by the plexin sema domain. *Neuron* **29**, 429–439 (2001).
29. Narazaki, M. & Tosato, G. Ligand-induced internalization selects use of common receptor neuropilin-1 by VEGF165 and semaphorin3A. *Blood* **107**, 3892–3901 (2006).
30. Nishikawa, K. *et al.* Maf promotes osteoblast differentiation in mice by mediating the age-related switch in mesenchymal cell differentiation. *J. Clin. Invest.* **120**, 3455–3465 (2010).
31. Gimble, J. M., Zvonic, S., Floyd, Z. E., Kassem, M. & Nuttall, M. E. Playing with bone and fat. *J. Cell. Biochem.* **98**, 251–266 (2006).
32. Krishnan, V., Bryant, H. U. & MacDougald, O. A. Regulation of bone mass by Wnt signaling. *J. Clin. Invest.* **116**, 1202–1209 (2006).
33. Takada, I., Kouzmenko, A. P. & Kato, S. Wnt and PPAR $\gamma$  signaling in osteoblastogenesis and adipogenesis. *Nature Rev. Rheumatol.* **5**, 442–447 (2009).
34. Toyofuku, T. *et al.* FARP2 triggers signals for *Sema3A*-mediated axonal repulsion. *Nature Neurosci.* **8**, 1712–1719 (2005).
35. Wu, X. *et al.* Rac1 activation controls nuclear localization of  $\beta$ -catenin during canonical Wnt signaling. *Cell* **133**, 340–353 (2008).
36. Takegahara, N. *et al.* Integral roles of a guanine nucleotide exchange factor, FARP2, in osteoclast podosome rearrangements. *FASEB J.* **24**, 4782–4792 (2010).
37. Nagashima, M. *et al.* Bisphosphonate (YM529) delays the repair of cortical bone defect after drill-hole injury by reducing terminal differentiation of osteoblasts in the mouse femur. *Bone* **36**, 502–511 (2005).
38. Tang, Y. *et al.* TGF- $\beta$ 1-induced migration of bone mesenchymal stem cells couples bone resorption with formation. *Nature Med.* **15**, 757–765 (2009).
39. Hayden, J. M., Mohan, S. & Baylink, D. J. The insulin-like growth factor system and the coupling of formation to resorption. *Bone* **17**, S93–S98 (1995).
40. Kawai, M., Mödder, U. I., Khosla, S. & Rosen, C. J. Emerging therapeutic opportunities for skeletal restoration. *Nature Rev. Drug Discov.* **10**, 141–156 (2011).
41. Grigoriadis, A. E. *et al.* c-Fos: a key regulator of osteoclast-macrophage lineage determination and bone remodeling. *Science* **266**, 443–448 (1994).
42. Asagiri, M. *et al.* Autoamplification of NFATc1 expression determines its essential role in bone homeostasis. *J. Exp. Med.* **202**, 1261–1269 (2005).
43. Mizuno, A. *et al.* Severe osteoporosis in mice lacking osteoclastogenesis inhibitory factor/osteoprotegerin. *Biochem. Biophys. Res. Commun.* **247**, 610–615 (1998).
44. Kaifu, T. *et al.* Osteopetrosis and thalamic hypomyelination with synaptic degeneration in DAP12-deficient mice. *J. Clin. Invest.* **111**, 323–332 (2003).
45. Hayashi, M. *et al.* Ly49Q, an ITIM-bearing NK receptor, positively regulates osteoclast differentiation. *Biochem. Biophys. Res. Commun.* **393**, 432–438 (2010).
46. Subramanian, A. *et al.* Gene set enrichment analysis: a knowledge-based approach for interpreting genome-wide expression profiles. *Proc. Natl Acad. Sci. USA* **102**, 15545–15550 (2005).

**Supplementary Information** is linked to the online version of the paper at [www.nature.com/nature](http://www.nature.com/nature).

**Acknowledgements** We are grateful to D. D. Ginty and A. L. Kolodkin for providing the *Nrp1*<sup>Sema-</sup> knockin mice. We thank Y. Goshima for providing vectors and technical help. We thank A. Yamaguchi, H. Asahara and F. Suto for providing reagents and technical help. We also thank K. Okamoto, T. Negishi-Koga, K. Nishikawa, H. Inoue, T. Suda, T. Ando, Y. Kunisawa, Y. Ogihara and S. Fukuse for discussion and assistance. This work was supported in part by a grant for the Exploratory Research for Advanced Technology Program, the Takayanagi Osteonetwork Project from the Japan Science and Technology Agency; Grant-in-Aid for Young Scientist A from the Japan Society for the Promotion of Science (JSPS); a Grant-in-Aid for Challenging Exploratory Research from the JSPS; grants for the Global Center of Excellence Program from the Ministry of Education, Culture, Sports, Science and Technology of Japan; and grants from the Tokyo Biochemical Research Foundation, the Life Science Foundation of Japan, Takeda Science Foundation, Uehara Memorial Foundation, Naito Foundation, BMKK RA Research Fund and Astellas Foundation for Research on Metabolic Disorders.

**Author Contributions** M.H. performed most of the experiments, interpreted the results and prepared the manuscript. T.N. performed immunohistochemical experiments and provided advice on project planning and data interpretation and prepared the manuscript. M.T. provided technical help. T.K. conducted the GeneChip analysis. A.K. provided advice on project planning and technical help. H.T. directed, supervised the project and wrote the manuscript.

**Author Information** Reprints and permissions information is available at [www.nature.com/reprints](http://www.nature.com/reprints). The authors declare no competing financial interests. Readers are welcome to comment on the online version of this article at [www.nature.com/nature](http://www.nature.com/nature). Correspondence and requests for materials should be addressed to H.T. ([taka.csi@tmd.ac.jp](mailto:taka.csi@tmd.ac.jp)).

## METHODS

**Cell culture.** For *in vitro* osteoclast differentiation in the monoculture system, primary bone marrow cells ( $1 \times 10^5$  cells per  $\text{cm}^2$ ) were suspended in culture medium ( $\alpha$ -MEM containing penicillin, streptomycin and 10% FBS) supplemented with  $10 \text{ ng ml}^{-1}$  M-CSF (R&D Systems) for two days to obtain BMMs. The resultant BMMs were further cultured in medium supplemented with  $10 \text{ ng ml}^{-1}$  M-CSF and  $5\text{--}50 \text{ ng ml}^{-1}$  RANKL (PeproTech) for three days. Culture medium was changed every second day. Where indicated, calvarial cell-conditioned medium with or without soluble Nrp1 (R&D Systems) was added 12 h before the RANKL stimulation. Sema3A-Fc (R&D Systems) was added 12 h before or 12 h after the RANKL stimulation. For Sema6D treatment, BMMs were collected and seeded onto culture plates coated with soluble recombinant Sema6D (R&D Systems), and cultured with  $10 \text{ ng ml}^{-1}$  M-CSF and  $5 \text{ ng ml}^{-1}$  RANKL for three days. For the generation of osteoclast *in vitro* in the coculture system, primary bone marrow cells ( $5 \times 10^4$  cells per  $\text{cm}^2$ ) and calvarial cells ( $5 \times 10^3$  cells per  $\text{cm}^2$ ) were cultured in the presence of  $10 \text{ nM}$   $1\alpha,25\text{-dihydroxyvitamin D}_3$  and  $1 \mu\text{M}$  prostaglandin E2 for 4–6 days. For human osteoclast differentiation, human peripheral blood mononuclear cells were separated from peripheral blood obtained from healthy volunteers by density gradient centrifugation with Lymphoprep (AXIS-SHIELD). Cells ( $2 \times 10^5$  cells per 0.5 ml) were cultured in  $\alpha$ -MEM with 10% FBS supplemented with  $30 \text{ ng ml}^{-1}$  M-CSF for two days. The resultant preosteoclasts were further cultured in medium supplemented with  $30 \text{ ng ml}^{-1}$  M-CSF and  $60 \text{ ng ml}^{-1}$  RANKL for four days. Culture medium was changed every second day. The differentiation of osteoclasts was evaluated by TRAP staining. A NF- $\kappa$ B activation inhibitor (6-amino-4-(phenoxyphenylethylamino)quinazoline; Calbiochem) was used to inhibit NF- $\kappa$ B activity. The concentration of intracellular calcium was measured as described<sup>27</sup>. For *in vitro* osteoblast differentiation, calvarial cells were isolated from the calvarial bone of newborn mice by enzymatic digestion in  $\alpha$ -MEM with 0.1% collagenase and 0.2% dispase, and were cultured with  $\alpha$ -MEM with 10% FBS. After two days, cells were reseeded ( $1 \times 10^4$  cells per  $\text{cm}^2$ ) and cultured with osteogenic medium (100 mM ascorbic acid, 5 mM  $\beta$ -glycerophosphate and 10 nM dexamethasone). Culture medium was changed every third day. After seven days, ALP staining and activity measurement were performed, and after 21 days, bone nodule formation was assessed by alizarin red staining. Human mesenchymal stem cells (Lonza) were cultured according to the manufacturer's protocol. To induce adipocyte differentiation *in vitro*, primary bone marrow cells ( $5 \times 10^5$  cells per  $\text{cm}^2$ ) were cultured with  $\alpha$ -MEM containing 10% FBS. After 24 h, non-adherent cells were removed and adherent cells were cultured with adipogenic medium (0.5 mM 3-isobutyl-1-methylxanthine,  $5 \mu\text{g ml}^{-1}$  insulin and  $1 \mu\text{M}$  dexamethasone) for 10–14 days. Culture medium was changed every second day. Lipid accumulation in adipocytes was determined with Oil Red O staining. Cell proliferation was determined using a cell proliferation ELISA kit (Roche Applied Science). The percentage of apoptotic cells was determined by TUNEL (TdT-mediated dUTP nick end labelling) staining with the MEBSTAIN apoptosis kit direct (MBL). For colony forming unit (CFU) assays, primary bone marrow cells ( $2.5 \times 10^5$  cells per  $\text{cm}^2$ ) were seeded and cultured with MesenCult basal medium supplemented with mesenchymal stem cell stimulatory supplements (StemCell Technologies). On day 10, the cells were stained with toluidine blue. For CFU-ALP and CFU-osteoblast (CFU-OB) assays, primary bone marrow cells ( $2.5 \times 10^5$  cells per  $\text{cm}^2$ ) were seeded and cultured with MesenCult basal medium and mesenchymal stem cell stimulatory supplements plus 100 mM ascorbic acid, 5 mM  $\beta$ -glycerophosphate and 10 nM dexamethasone. On day 10, CFU-ALP colonies were stained for ALP. Mineral deposition was determined with von Kossa staining of CFU-OB colonies on day 25. Primary osteoblasts and osteocytes were isolated from the long bones of CAG-CAT-EGFP/Dmp1-Cre double transgenic mice as described<sup>11</sup>.

**Purification and identification of inhibitory factor of osteoclast differentiation.** Mouse calvarial cells were statically cultured with  $\alpha$ -MEM supplemented with 1% FBS. Medium was conditioned for 72 h and filtered to remove non-adherent cells and debris. Conditioned medium was concentrated by ammonium sulphate precipitation (40% saturation), and the pellet was suspended in 10 mM sodium phosphate buffer, pH 7.4, and desalted using a PD-10 column (GE Healthcare). Concentrated conditioned media were then loaded onto a Mono Q 5/50 column (GE Healthcare) in 10 mM sodium phosphate buffer, pH 7.4, and proteins binding to the Mono Q matrix were eluted by a gradient of 0–100% 1 M NaCl and 10 mM sodium phosphate buffer, pH 7.4. Protein concentrations were determined by the absorbance at 280 nm. The effect of the fractionated conditioned media on osteoclast differentiation was examined by directly adding each fraction to RANKL-induced osteoclast differentiation *in vitro*. Fractions 33–35 contained a high concentration of NaCl, which exerts an inhibitory effect on osteoclast differentiation. Proteins of the highly inhibitory fractions were dissolved in SDS-PAGE sample buffer (Nacalai Tesque) and the sample was resolved by SDS-PAGE. Protein bands were visualized by Coomassie brilliant blue staining and all the protein bands were excised by scalpel. The samples were

analysed using nano-LC-MS/MS by Japan Bioservice. The data were submitted to the MASCOT program for identification.

**Immunohistochemical staining.** After fixation in 4% paraformaldehyde, bone tissues were decalcified in 10% EDTA at 4 °C for 2 weeks and embedded in paraffin after dehydration. For immunohistochemical staining, antigen retrieval was carried out with 10 mM citric acid, pH 6.0, at room temperature for 2 h. After quenching of endogenous peroxidase activity by incubation with 3%  $\text{H}_2\text{O}_2$  in methanol, the sections were incubated with an anti-Sema3A polyclonal antibody (Santa Cruz Biotechnology) in immunoreaction enhancer solution (Can Get Signal immunostain, TOYOCO) at 4 °C for overnight. After washing with PBS, the sections were incubated with peroxidase-conjugated secondary antibody according to the manufacturer's instructions (histofine, Nichirei Bioscience). The signals were visualized with 3,3'-diaminobenzidine tetrahydrochloride and  $\text{H}_2\text{O}_2$ . TRAP staining was conducted after the immunostaining. Haematoxylin was used for nuclear counterstaining.

**Western blot and immunoprecipitation analyses.** Cell lysate or culture supernatant of calvarial cells was subjected to western blot analysis using the specific antibodies for Nrp1 (Calbiochem),  $\beta$ -actin (Sigma-Aldrich), Sema3A, Nrp1, p50, p65, histone H1 (Santa Cruz Biotechnology), phospho-ERK, ERK, phospho-JNK, JNK, phospho-p38, p38, phospho- $\text{IKK}\alpha/\beta$ ,  $\text{IKK}\alpha$ ,  $\text{IKK}\beta$ , phospho-PLC $\gamma$ 2, PLC $\gamma$ 2 (Cell Signaling Technology),  $\beta$ -catenin (Millipore) and  $\alpha$ -tubulin (MBL). Nuclear proteins were prepared with nuclear extract kit in accordance with the manufacturer's protocol (Active Motif). For immunoprecipitation analysis, cells were solubilized in lysis buffer (1% Nonidet P-40 in 50 mM NaCl, 50 mM Tris-HCl, 5 mM EDTA, 1 mM NaF and 2 mM PMSF), supplemented with complete protease inhibitor cocktail (Roche Applied Science). Immunoprecipitation was performed by incubation with an anti-Flag M2 (Sigma-Aldrich) or anti-PlxnA1 antibody (Santa Cruz Biotechnology) followed by the addition of dynabeads protein G (Invitrogen). Immune complexes were separated by electrophoresis followed by blotting with anti-Flag M2, anti-V5 (Invitrogen), anti-Nrp1, anti-PlxnA1, anti-DAP12 (Santa Cruz Biotechnology) and anti-TREM2 antibodies (R&D Systems).

**Flow cytometric analysis.** For the analysis of bone marrow-derived osteoclast precursor cells, a single cell suspension of mouse bone marrow cells was stained with anti-CD3e (145-2C11, eBioscience), anti-B220 (RA3-6B2, eBioscience), anti-CD11b (M1/70, eBioscience), anti-CD115 (AFS98, eBioscience) and anti-CD117 (2B8, eBioscience) antibodies. For intracellular staining of BMMs, anti-CD11b and anti-Nrp1 and anti-Nrp1 (R&D Systems) were used. Flow cytometric analysis was performed using FACSCantoII with Diva software (BD Biosciences).

**ELISA.** Concentrations of soluble RANKL and Opg in serum were determined using ELISA kits (R&D Systems), according to the manufacturer's instruction.

**Retroviral gene transfer.** The retroviral vector pMXs-Nrp1-IRES-EGFP was constructed by inserting DNA fragments encoding Nrp1 into pMXs-IRES-EGFP. The construction of the retroviral vectors pMX-FARP2-IRES-GFP and pMX-AGEF-FARP2-IRES-GFP was described previously<sup>36</sup>. For the construction of the retroviral vectors pSIREN-RetroQ-ZsGreen-shNrp1 and pSIREN-RetroQ-ZsGreen-shControl, RNA targeting regions with a hairpin sequence (Nrp1 shRNA sense: 5'-GCCCGAATGTTCTCAGAAGCTACTCGAGTAGTCTGAGAATTCGGGCTTTT-3'; Nrp1 shRNA antisense: 5'-AAAAAGCCCGAATGTTCTCAGAAGCTACTCGAGTAGTCTGAGAATTCGGGCTTTT-3'; control shRNA sense: 5'-GTGCGTTGCTAGTACCACTTCAAGATTCTTTTACGCT-3'; control shRNA antisense: 5'-ACGCGTAAAAATCTCTTGAAGTTGGTACTAGCAACGACAC-3') were inserted into RNAi-ready pSIREN-RetroQ-ZsGreen (Clontech). The retrovirus supernatants were obtained by transfecting the retroviral vectors into the Plat-E packaging cell line using FuGENE 6 (Roche Applied Science).

**Chromatin immunoprecipitation assay.** Chromatin immunoprecipitation assay was performed using the CHIP-IT express chromatin immunoprecipitation kit (Active Motif) according to the manufacturer's instructions. The antibodies used for immunoprecipitation were anti-p50, anti-p65 and normal rabbit IgG (Santa Cruz Biotechnology). The primer sequences were as follows: Nrp1 region 1, 5'-CATACGTGACCTTGGCTCT-3' and 5'-CCTGGCTGGAGATTCAGA G-3'; Nrp1 region 2, 5'-ACCTTACCACCAGCTCCTT-3' and 5'-ATACGCCACCACTTACGAG-3'; Nrp1 region 3, 5'-ATGTGGCTTGGTGAAAG GAG-3' 5'-TGCTTCTACCTTCGGGTGAT-3'.

**Reporter gene assay.** The reporter plasmid Nrp1-Luc was constructed by subcloning a 3,259 base pair fragment of the 5' flanking region of the mouse Nrp1 gene into the pGL3-basic vector (Promega). The reporter plasmids and the expression plasmids were transfected into NIH3T3 cells using FuGENE 6 (Roche Applied Science). After 36 h, dual luciferase assay was performed according to the manufacturer's protocol (Promega).

**Migration assay.** BMMs suspended in complete medium were added to the upper chamber of transwell units (Corning). Inserts were placed into the lower chambers

of transwell units containing M-CSF with or without Sema3A-Fc. After incubation, cells were fixed with 4% paraformaldehyde and stained with 0.5% toluidine blue. The cells on the upper side of the membrane were removed and the cells that had migrated to the lower side of the membrane and chamber were counted.

**G-LISA small G protein activation assay.** RhoA and Rac GTPase activation were determined using the G-LISA RhoA and Rac absorbance-based assay (Cytoskeleton) according to the manufacturer's instructions. In brief, cell lysates were prepared and normalized. After the addition of antibodies against RhoA or Rac and the incubation with the horseradish peroxidase detection reagent, signals were detected with a spectrophotometer.

**In vivo treatment with recombinant Sema3A.** Five-week-old C57BL/6 mice were given weekly intravenous injections of 1 mg per kg body weight of Sema3A-Fc or vehicle for four weeks. Three days after the last injection, bone analysis was performed as described earlier.

**Bone regeneration model.** Skeletal injury was generated as described previously<sup>37</sup>. In brief, C57BL/6 mice were anaesthetized with an intraperitoneal

injection of pentobarbital sodium. A 5-mm longitudinal incision was made over the proximal femur and the bone surface was exposed by splitting the muscle. A 0.5-mm hole was made by drilling through the anterior portion of the diaphysis of the bilateral femurs. After four and seven days of surgery, femoral defects were treated with Sema3A-Fc (0.5 mg per kg body weight) by injection into the injury site. Mice were euthanized at day 14 after surgery and bone analyses were performed.

**Ovariectomy-induced bone loss.** Nine-week-old female mice were ovariectomized or sham operated. More than five mice were examined in each group. Ovariectomized mice were given weekly intravenous injections of 1 mg per kg body weight of Sema3A-Fc or vehicle for four weeks. Three days after the last injection, all of the mice were euthanized and subjected to bone analysis as described earlier.

**Statistical analyses.** Statistical analyses were performed using the unpaired two-tailed Student's *t* test (\**P* < 0.05; \*\**P* < 0.01; \*\*\**P* < 0.001; NS, not significant, throughout the paper). All data are expressed as the mean ± s.e.m. Results are representative examples of more than three independent experiments.